Chapter 6
Monotonic and Cyclic Loading Processes

Valentin S. Bondar and Dmitry R. Abashev

Abstract Experimental analysis of 12X18H10T stainless steel specimens subjected to strain-controlled cyclic loading that comprises sequential monotonic and cyclic loading under uniaxial tension-compression and standard temperature is used to identify some features and dissimilarities of isotropic and anisotropic hardening processes that occur during monotonic and cyclic loading. In order to describe these features in terms of the plasticity theory (the Bondar model), which can be classified as a combined-hardening flow theory, plastic-strain redirection criterion and the memory surface concept are introduced in the plastic-strain tensor space so as to separate monotonic and cyclic strain. Evolution equations for isotropic and anisotropic hardening processes are derived to describe the monotonic-to-cyclic and cyclic-to-monotonic evolutions in transients. The basic experiment used to determine the material functions consists of three stages: cyclic loading, monotonic loading, and subsequent cyclic loading until fracture. The results of the basic experiment are fundamental to the proposed method for identifying the material functions. Basic-experiment results and the identification method are used to identify the room-temperature material functions of 12X18H10T stainless steel. The paper compares the computational analysis and the experimental analysis of stainless steel subjected to a strain-controlled fatigue test (loading) in five stages: cyclic, monotonic, cyclic, monotonic, and cyclic loading until fracture. It further compares the computational and experimental kinetics of the stress-strain state throughout the deformation process. Changes in the amplitude and mean cycle stress during the cyclic stress stages are subsequently analyzed. These stages are characterized by hysteresis loop stabilization. Computational and experimental results fit reliably. The theory adequately describes the processes of how the kinetics, the amplitudes, and the mean cycle stress alter when subjecting a specimen to strain-controlled loading, which enables a more adequate description of stress-controlled loading, especially when loading is non-stationary and non-symmetric.

V. S. Bondar · D. R. Abashev (✉)
Department of Technical Mechanics, Moscow Polytechnic University, Moscow 107023, Russian Federation
e-mail: tm@mospolytech.ru

H. Altenbach et al. (eds.), *Deformation and Destruction of Materials and Structures Under Quasi-static and Impulse Loading*, Advanced Structured Materials 186,
https://doi.org/10.1007/978-3-031-22093-7_6

Keywords Experiment · Strain-controlled cyclic loading · Plasticity · Combined-hardening flow theory

6.1 Introduction

Non-stationary asymmetric cyclic strain is a deformation process that is a sequence of monotonic and cyclic loadings. It is a very complex problem to model such processes mathematically when subjecting a specimen to strain-controlled cyclic loading, even more so in the case of stress-controlled loading. Besides, such loadings are associated with the hard-to-model hysteresis loop ratcheting and stabilization. As for the assessment and prediction of the resource under non-stationary and asymmetric cyclic loading conditions, fatigue damage accumulation must be determined throughout the deformation process given the significant non-linearity of such damage.

Mathematical modeling of strain and damage accumulation when subjecting a specimen to cyclic loading is mainly based on variants of plasticity theories belonging to the class of combined (isotropic and anisotropic) hardening plastic-flow theories as reviewed and analyzed in [1, 2, 4–12, 14–34, 37–40]. In this paper, such modeling is based on the Bondar model, a version of plasticity theory [7–9, 11, 12] (Bondar et al., 2013) which, as shown in [13], is the most adequate version for describing cyclic loading-induced strain and fracture, as compared to the Korotkikh [21, 25, 33–35] or Chaboche [6, 14, 18] models. This paper presents the basic equations of the Bondar Model.

In order to identify the features of strain induced by non-stationary and asymmetric cyclic loading, strain-controlled loading is analyzed by subjecting 12X18H10T stainless steel specimens to tension–compression tests in a sequence of five stages: cyclic, monotonic, cyclic, monotonic, and cyclic loading until fracture. Analysis of the cyclic-to-monotonic and monotonic-to-cyclic transients shows the need to separate the monotonic and the cyclic deformation processes. To that end, a plastic-strain redirection criterion and the memory surface concept for separating the monotonic and cyclic deformation processes are introduced in the plastic-strain space. Evolution equations of isotropic and anisotropic hardening parameters for monotonic and cyclic loading are further introduced in the Bondar plasticity theory equations.

Separation of the monotonic and cyclic strain is also a feature of the Korotkikh model [34], where it is only used to describe the evolution of isotropic hardening. The memory surface in this model is constructed in the backstress deviator space while determining the maximum backstress intensity value in the deformation process. In [25, 34], the evolution of anisotropic hardening in a plastic-strain deviator space is described by introducing a memory surface while determining the maximum plastic-strain intensity amplitude in the deformation process. The paper [36] uses the same memory surface to describe the anisotropic hardening evolution as in the case of isotropic hardening. All these approaches [25, 34, 36] have one significant drawback: the resulting memory surface size can potentially decrease and increase at the end of the cycle, resulting in a chance of it either both monotonic or cyclic loading at the

end of each cycle. Besides, the evolution equation for the maximum cyclic loading backstress intensity means that this value is always diminishing, although it should remain constant in a stabilized cycle. In conclusion, it should also be noted that there is no documented adequate rationale for the considered approaches [25, 34, 36].

Taking into account the identified features of monotonic and cyclic loading for the refined equations of the modified Bondar plasticity theory, this research has defined the basic experiment as well as the method for identifying the material functions. The material functions of 12H18N10T stainless steel at room temperature are obtained. This paper compares the computational analysis and experimental analysis of 12H18N10T stainless steel subjected to strain-controlled loading that is a sequence of monotonic and cyclic loadings. The kinetics of the stress–strain state is analyzed, and changes in the amplitude and mean stress of the cycle during the cyclic loading stages are taken into account.

6.2 Basic Equations of the Plasticity Theory

A simplified version of the plasticity theory [10, 11, 13], which is a partial version of the theory of inelasticity [7, 9], is considered. This version is a single-surface combined-hardening flow theory. Its applicability is limited to small strains of initially isotropic metals at temperatures that entail no phase transformations, at such strain rates where dynamic and rheological effects are negligible.

Below is a summary of the basic equations for this plasticity theory version.

1. $\dot{\varepsilon}_{ij} = c + \dot{\varepsilon}^p_{ij}$.
2. $\dot{\varepsilon}^e_{ij} = \frac{1}{E}\left[\dot{\sigma}_{ij} - \nu\left(3\dot{\sigma}_0\delta_{ij} - \dot{\sigma}_{ij}\right)\right]$.
3. $f\left(\sigma_{ij}\right) = \frac{3}{2}\left(s_{ij} - a_{ij}\right)\left(s_{ij} - a_{ij}\right) - C^2 = 0$.
4. $\dot{C} = q_\varepsilon \dot{\varepsilon}^p_{u^*}, \quad \dot{\varepsilon}^p_{u*} = \left(\frac{2}{3}\dot{\varepsilon}^p_{ij}\ \dot{\varepsilon}^p_{ij}\right)^{\frac{1}{2}}$.
5. $\dot{a}_{ij} = \sum\limits_{m=1}^{M} \dot{a}^{(m)}_{ij}$.
6. $\dot{a}^{(1)}_{ij} = \frac{2}{3}g^{(1)}\dot{\varepsilon}^p_{ij} + g^{(1)}_a a^{(1)}_{ij}\dot{\varepsilon}^p_{u*}$.
7. $\dot{a}^{(2)}_{ij} = \frac{2}{3}g^{(2)}\dot{\varepsilon}^p_{ij} + g^{(2)}_a a^{(2)}_{ij}\dot{\varepsilon}^p_{u*}$.
8. $\dot{a}^{(m)}_{ij} = \frac{2}{3}g^{(m)}\dot{\varepsilon}^p_{ij} \quad (m = 3, ..., M)$.
9. $\dot{\varepsilon}^p_{ij} = \frac{\partial f}{\partial \sigma_{ij}}\lambda = \frac{3}{2}\frac{s^*_{ij}}{\sigma^*_u}\dot{\varepsilon}^p_{u*}, \quad s^*_{ij} = s_{ij} - a_{ij}, \qquad \sigma^*_u = \left(\frac{3}{2}s^*_{ij}\, s^*_{ij}\right)^{\frac{1}{2}}$.
10. $\dot{\varepsilon}^p_{u^*} = \frac{1}{E_*}\frac{3}{2}\frac{s^*_{ij}\dot{\sigma}_{ij}}{\sigma^*}, \quad E_* = q_\varepsilon \sum\limits_{m=1}^{M} g^{(m)} + \sum\limits_{m=1}^{2} g^{(m)}_a a^{(m)*}_u, \quad a^{(m)*}_u = \frac{3}{2}\frac{s^*_{ij}a^{(m)}_{ij}}{\sigma^*_u}$
11. $\dot{\varepsilon}^p_{u^*} = \frac{1}{E_* + 3G}\, 3\, G\frac{s^*_{ij}}{\sigma^*}\frac{\dot{\varepsilon}_{ij}}{}, \quad G = \frac{E}{2(1+\nu)}$.
12. $\sigma^*_u < C \cup \dot{\varepsilon}^p_{u*} \le 0$—elasticity,
    $\sigma^*_u = C \cap \dot{\varepsilon}^p_{u*} > 0$—elastoplasticity.
13. $\dot{\omega} = \alpha\omega^{\frac{\alpha-1}{\alpha}}\frac{a^{(2)}_{ij}\dot{\varepsilon}^p_{ij}}{W_a}, \qquad \alpha = \left(\sigma^{(2)}_a / a^{(2)}_u\right)^{n_\alpha}, \quad a^{(2)}_u = \left(\frac{3}{2}a^{(2)}_{ij}\ a^{(2)}_{ij}\right)^{\frac{1}{2}}$.

Here, $\dot{\varepsilon}_{ij}$, $\dot{\varepsilon}^e_{ij}$, $\dot{\varepsilon}^p_{ij}$ are the total, elastic, and plastic-strain rate tensors; σ_{ij}, s_{ij}, s^*_{ij}, a_{ij} is the stress tensor, stress, active-stress, and backstress deviators; ε^p_{u*} is the accumulated plastic strain; ω is the damage; E, ν are Young's modulus and Poisson's ratio; C is the radius (size) of the yield surface; $a^{(1)}_{ij}$, $a^{(2)}_{ij}$, $a^{(m)}_{ij}$ are Type I, II, and III backstresses (yield surface center displacement deviator); and q_ε, $g^{(m)}$, $g^{(m)}_a$ are the defining functions, the relationship whereof to the material functions is described below.

6.3 Monotonic and Cyclic Loading of 12X18H10T Stainless Steel

The paper presents the results of experimenting with 12X18H10T stainless steel subjected to uniaxial strain-controlled loading, which is a sequence of monotonic and cyclic loading stages. The experiment consists of five loading stages:

- Stage 1 involves cyclic loading at $\varepsilon^{(1)}_m = 0$, $\Delta\varepsilon^{(1)} = 0.016$, and $N^{(1)} = 20$ cycles;
- Stage 2 involves monotonic tension test up to $\varepsilon^{(2)} = 0.05$;
- Stage 3 involves cyclic loading at $\varepsilon^{(3)}_m = 0.05$, $\Delta\varepsilon^{(3)} = 0.012$, and $N^{(3)} = 200$ cycles;
- Stage 4 involves monotonic tension up to $\varepsilon^{(4)} = 0.1$;
- Stage 5 involves cyclic loading at $\varepsilon^{(5)}_m = 0.1$, $\Delta\varepsilon^{(5)} = 0.012$, and $N^{(5)} = N_f$ cycles until fracture.

Here, $\varepsilon^{(i)}_m$ is the mean cycle strain; $\Delta\varepsilon^{(i)}$ is the cycle strain amplitude; $\varepsilon^{(i)}$ is the final monotonic strain; $N^{(i)}$ is the number of cycles.

Figure 6.1 shows the experimental diagram of the 12X18H10T steel strain that covers all five loading stages. The cyclic diagrams of Stages I, II, and III show the loops for the first cycle and the last cycle. Experimental results are analyzed below.

Cyclic deformation at Stage I entails a cyclical hardening of 12X18H10T steel at the initial stage, which slows down to insignificant levels $\left(dC_p/d\varepsilon^p_{u*} \approx 1\,\mathrm{M}\prod \mathrm{a}\right)$; then the steel becomes virtually cyclically stable.

Stages III and V feature stabilization of the hysteresis loop. These stages are identical stabilization-wise, as if there was no pre-history of strain. Thus, the modulus E_a, which is part of the Type I backstress evolution equation and is necessary for loop stabilization, must have the same initial value $E_a = E_{a0}$. That said, during monotonic post-cyclic loading, when E_a is reduced to nearly zero, the modulus E_a must quickly return to its initial value E_{a0}.

Hardening is constant at Stages II and IV of monotonic loading. Here, hardening is determined by the modulus E_{a0} and to a lesser extent by the modulus of monotonic isotropic hardening.

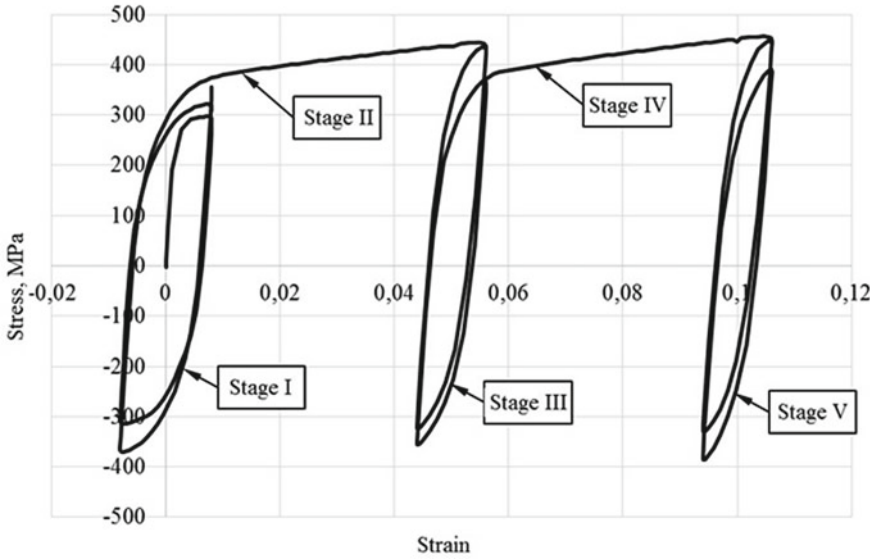

Fig. 6.1 Stress–strain diagram of 12X18H10T steel

Thus, the behavior of the modulus E_a that describes the anisotropic hardening, and therefore the behavior of the isotropic hardening parameters, will depend significantly on whether the strain is cyclic or monotonic.

Memory surface that limits the cyclic deformation area is introduced in the plastic-strain tensor space ε_{ij}^{p} in order to separate monotonic and cyclic strain. The surface is determined by the position of its center ξ_{ij} and its radius (size) C_{ε}. To compute the center and size of the surface, two plastic-strain tensors $\varepsilon_{ij}^{p(1)}$ and $\varepsilon_{ij}^{p(2)}$ are introduced to define the surface boundaries. These variables are zero as strain begins. The displacement and size of the memory surface are determined at the time plastic strain is redirected. The following condition is assumed as the redirection criterion:

$$\dot{\varepsilon}_{ij(t-0)}^{p}\dot{\varepsilon}_{ij(t)}^{p} < 0, \tag{6.1}$$

where $\dot{\varepsilon}_{ij(t)}^{p}$ is the current plastic-strain rate tensor; $\dot{\varepsilon}_{ij(t-0)}^{p}$ is the plastic-strain rate tensor at the preceding time point.

At this moment, the change in the boundaries, center, and size of the yield surface is described based on the following relationships:

$$\varepsilon_{ij}^{p(2)} = \varepsilon_{ij}^{p(1)}, \tag{6.2}$$

$$\varepsilon_{ij}^{p(1)} = \varepsilon_{ij}^{p}, \tag{6.3}$$

$$\xi_{ij} = \frac{\varepsilon_{ij}^{p(1)} + \varepsilon_{ij}^{p(2)}}{2}, \tag{6.4}$$

$$C_\varepsilon = \left[\frac{2}{3}\left(\frac{\varepsilon_{ij}^{p(1)} - \varepsilon_{ij}^{p(2)}}{2}\right)\left(\frac{\varepsilon_{ij}^{p(1)} - \varepsilon_{ij}^{p(2)}}{2}\right)\right]^{\frac{1}{2}}. \tag{6.5}$$

Then the condition of cyclic strain is the strain within the memory surface

$$\left[\frac{2}{3}\left(\varepsilon_{ij}^{p} - \xi_{ij}\right)\left(\varepsilon_{ij}^{p} - \xi_{ij}\right)\right]^{\frac{1}{2}} \le C_\varepsilon \tag{6.6}$$

Outside the memory surface, the strain is monotonous.

Based on the above peculiarities of monotonic and cyclic loading, the following equations are derived for the modulus E_a and backstress defining functions:

$$g^{(1)} = E_a,\ g^{(2)} = \beta^{(2)}\sigma_a^{(2)},\ g_a^{(2)} = -\beta^{(2)}, \tag{6.7}$$

$$g^{(m)} = \begin{cases} \beta^{(m)},\ \sigma_a^{(m)}, \\ 0,\ \text{если}\ a_u^{(m)} \ge \sigma_a^{(m)} \bigcap a_{ij}^{(m)} s_{ij}^{*} > 0, \end{cases} \tag{6.8}$$

$$\begin{gathered} a_u^{(m)} = \left(\frac{3}{2} a_{ij}^{(m)} a_{ij}^{(m)}\right)^{\frac{1}{2}} \quad m = 3, ..., M \\ \dot{E}_a = \begin{cases} -K_E\left(\frac{E_a}{E_{a0}}\right)^{n_E} \dot{\varepsilon}_{u*}^{p} & \text{cyclic loading}, \\ M_E\left(\frac{E_{a0} - E_a}{E_{a0}}\right) \dot{\varepsilon}_{u*}^{p} & \text{monotonic loading}, \end{cases} \end{gathered} \tag{6.9}$$

$$g_a^{(1)} = \begin{cases} \frac{1}{E_a}\frac{d E_a}{d \varepsilon_{u*}^{p}} & \text{cyclic loading}, \\ 0 & \text{monotonic loading}. \end{cases} \tag{6.10}$$

Therefore, the following material functions need to be derived in order to describe backstresses:

E_{a0}, $\sigma_a^{(m)}$, $\beta^{(m)}$ are the moduli of anisotropic hardening;

K_E, n_E, M_E are the parameters of anisotropic hardening when subjecting the material to cyclic and monotonic strain.

The results of the experiment (Fig. 6.1) are used to define these material functions.

Anisotropic hardening modulus E_{a0} is found by the formula

$$E_{a0} = \frac{\sigma_m^{(3)}}{\varepsilon_m^{p(3)}}, \tag{6.11}$$

where $\sigma_m^{(3)}$ is the mean stress in the first Stage III cycle; $\varepsilon_m^{p(3)}$ is the mean plastic strain at the first cycle Stage III cycle.

The moduli of anisotropic hardening $\sigma_a^{(m)}$ and $\beta^{(m)}$ are found by processing the cyclic diagram of the last Stage I semi-cycle as per the procedure described in [10, 11].

The anisotropic hardening parameters K_E and n_E are found based on the results of the hysteresis loop stabilization at Stages III and V. To that end, the dependence in the coordinates

$$Y_E = \ln\left[\frac{\sigma_m(N-1) - \sigma_m(N)}{2\Delta\varepsilon^p\, \varepsilon_m^p}\right], \tag{6.12}$$

$$X_E = \ln\left[\frac{\sigma_m(N)}{\varepsilon_m^p\ E_{a0}}\right] \tag{6.13}$$

is constructed, where N is the cycle number; $\sigma_m(N)$ is the mean stress of the Nth cycle; $\Delta\varepsilon^p$ is the plastic-strain amplitude; ε_m^p is the mean plastic strain. The dependence obtained is approximated by the linear function

$$Y_E = a_E\, X_E + b_E. \tag{6.14}$$

Thus,

$$K_E = \exp(b_E), \quad n_E = a_E. \tag{6.15}$$

The parameter of anisotropic hardening M_E of a specimen subjected to monotonic loading is determined from the considerations of restoring the parameter E_a from 0 to the value E_{a0}, whereby plastic strain changes under monotonic loading over ε_{st}^p. Thus, the parameter M_E shall be determined by the formula

$$M_E = \frac{E_{a0}}{\varepsilon_{st}^p}. \tag{6.16}$$

Having found the backstresses over the entire process from Stage I to Stage V, one can determine the behavior of the yield surface size (radius), i.e. the change in isotropic hardening in cyclic-to-monotonic and monotonic-to-cyclic strain transients.

Figure 6.2 shows the change in the yield surface size (functional C) throughout the deformation process from Stage I to Stage V.

The dotted line in Fig. 6.2 shows the function of isotropic hardening $C = C_p\left(\varepsilon_{u*}^p\right)$ induced by cyclic loading. Analysis of the results, presented in Fig. 6.2, shows that the transition from cyclic to monotonic strain (Stages II and IV) is associated with an increase in the intensity of isotropic hardening. The transition from monotonic to cyclic strain (Stages III and V) is associated with a slowdown in such isotropic hardening, as it tends to be isotropic $C = C_p\left(\varepsilon_{u*}^p\right)$ when subjecting the specimen to cyclic strain.

Based on the above peculiarities of how isotropic hardening is altered by cyclic or monotonic loading, the following dependence is assumed for the defining function of isotropic hardening:

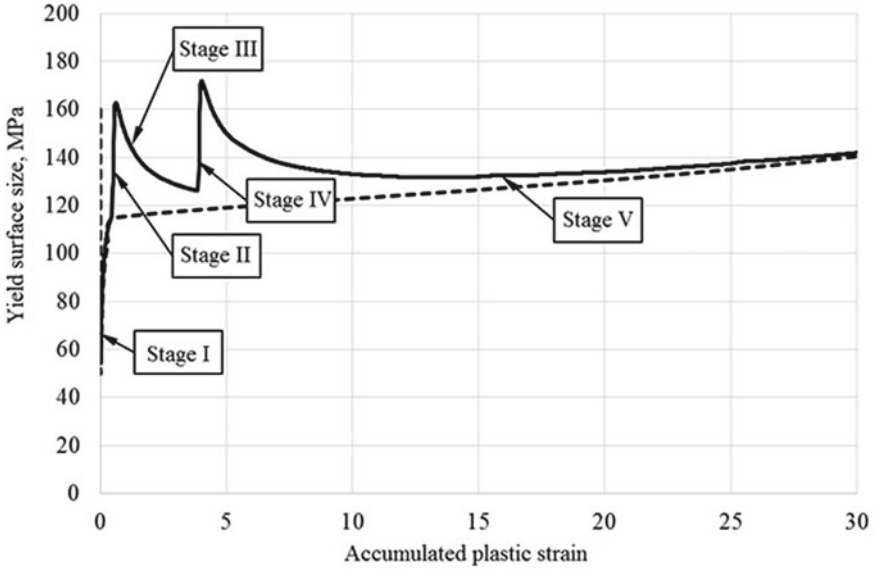

Fig. 6.2 Yield surface-size change

$$q_\varepsilon = \begin{cases} \left[\frac{dC_p}{d\varepsilon^p_{u*}} - K_C\left(\frac{C-C_p}{C_p}\right)^{n_C}\right] & \text{cyclic loading,} \\ \left[\frac{dC_p}{d\varepsilon^p_{u*}} + M_C\right] & \text{monotonic loading.} \end{cases} \tag{6.17}$$

Thus, to describe such isotropic hardening, the following material functions must be defined:

$C_p\left(\varepsilon^p_{u*}\right)$ is the function of isotropic hardening induced by cyclic loading;

K_C, n_C, M_C are the moduli of isotropic hardening induced by cyclic and monotonic loading.

These material functions are defined using the experiment results, see Fig. 6.2. The function of isotropic hardening induced by cyclic loading $C_p\left(\varepsilon^p_{u*}\right)$ is determined based on the surface-size changes at Stages III and V; see the dotted curve in Fig. 6.2 and I.

Cyclic loading isotropic hardening parameters K_C and n_C are found from the results of decreasing the yield surface size at Stages III and V. To that end, a dependence is constructed in the coordinates

$$Y_C = \ln\left[\frac{d\left(C_p - C\right)}{d\varepsilon^p_{u*}}\right], \tag{6.18}$$

$$X_C = \ln\left[\frac{\left(C - C_p\right)}{C_p}\right]. \tag{6.19}$$

Table 6.1 Material functions of 12X18H10T steel

E, MPa	ν	E_{a0}, MPa	$\sigma_a^{(2)}$,MPa	$\beta^{(2)}$	K_E, MPa	n_E	M_E, MPa	K_C, MPa	n_C	M_C, MPa
$2 \cdot 10^5$	0.3	800	140	260	$1,4 \cdot 10^4$	3.5	$4 \cdot 10^4$	148	1.4	960

$\sigma_a^{(3)}$, MPa	$\beta^{(3)}$	$\sigma_a^{(4)}$, MPa	$\beta^{(4)}$	$\sigma_a^{(5)}$, MPa	$\beta^{(5)}$	W_a, MJ/M^3	n_α
45	5000	41	2000	36	1100	1830	1.5

Table 6.2 Isotropic hardening function of 12X18H10T steel

ε_{u*}^p	0	0.0003	0.0006	0.0014		0.0045	0.006	0.01	0.025
C_p, MPa	160	125	110	100		65	50	51	57
ε_{u*}^p	0.1	0.15	0.3	0.45	0.6	1	8	25	45
C_p, MPa	85	90	105	110	115	115	121	135	159

The dependence obtained is approximated by the linear function

$$Y = a_C X_C + b_C \ . \tag{6.20}$$

Thus

$$K_C = \exp(b_C), \quad n_C = a_C. \tag{6.21}$$

The parameter of isotropic hardening M_C induced by monotonic strain is found from the slope of the strain curve at Stages II and IV using the formula

$$M_C = \frac{d\sigma}{d\varepsilon^p} - E_{a0} - \frac{dC_p}{d\varepsilon^p} \tag{6.22}$$

6.4 Material Functions of 12X18H10T Stainless Steel

Material functions have been derived based on the results of room-temperature experiments with 12X18H10T stainless steel; see Tables 6.1 and 6.2.

6.5 Verification of the Modified Plasticity Theory

To verify the modified plasticity theory, the researchers have computed the kinetics of the stress–strain state of 12X18H10T stainless steel subjected to strain-controlled cyclic and monotonic loading according to the five-stage program described in

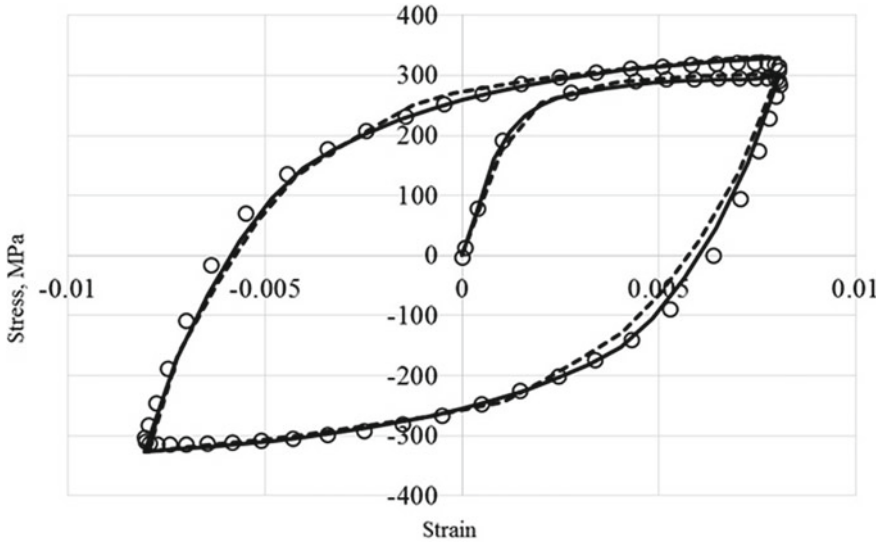

Fig. 6.3 First Stage I cycle

Section 6.2. Computation uses the material functions per Section 6.3. Figures 6.3, 6.4, 6.5, 6.6, and 6.7 present a comparison of the computed (solid curves) and experimental (open circles) results. The dotted curves show the results based on the variant [13] of the modified Bondar model. Figure 6.3 shows the cyclic diagram of the first Stage I cycle; Fig. 6.4 shows the 20th (last) Stage I cycle, the monotonous loading at Stage II, and the first Stage III cycle; Fig. 6.5 shows the 200th (last) Stage III cycle, the monotonous loading at Stage IV, and the first Stage V cycle. Variations in the stress amplitude and mean cycle stress at Stages I, III, and V are shown in Figs. 6.6 and 6.7.

There is a significant improvement in the description of the stress–strain state kinetics based on the variant proposed herein, as compared to the previously [13] modified model. As for the changes in the amplitude and mean stress of the cycles, the proposed version adequately describes these rather complex processes.

6.6 Conclusions

Analysis of the stainless steel experiments leads to a conclusion that the processes of isotropic and anisotropic hardening vary significantly depending on whether the strain is monotonic or cyclic. Monotonic-to-cyclic and cyclic-to-monotonic strain transitions are associated with hardening transients.

In the light of the identified features of monotonic and cyclic loading, the equations of the modified Bondar plasticity theory have been refined. The researchers

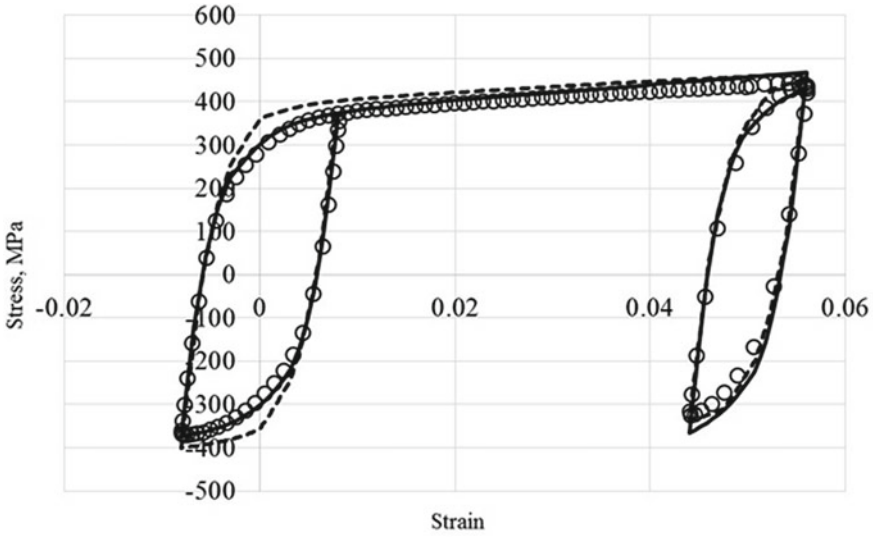

Fig. 6.4 Last Stage I cycle, Stage II, and first Stage III cycle

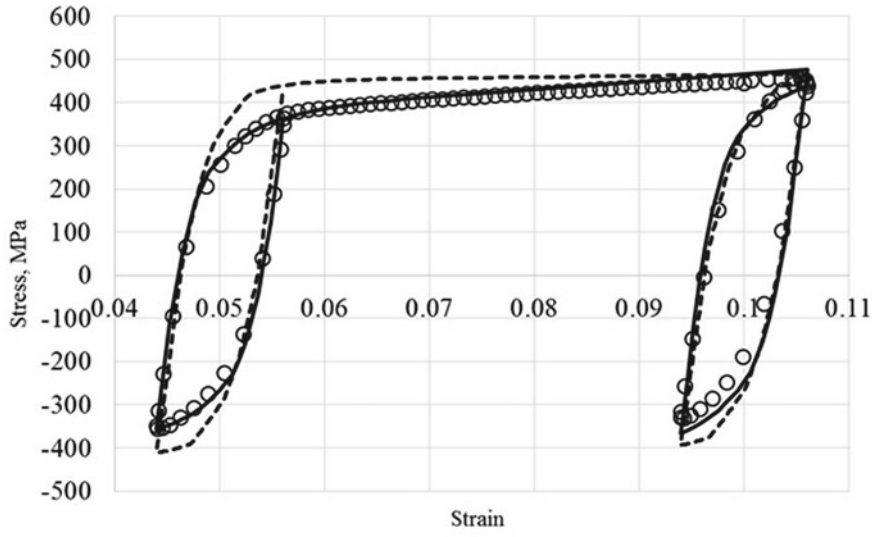

Fig. 6.5 Last Stage III cycle, Stage IV, and first Stage V cycle

have defined the basic experiment, derived the material-function identification method, and obtained such material functions for 12X18H10T stainless steel at room temperature.

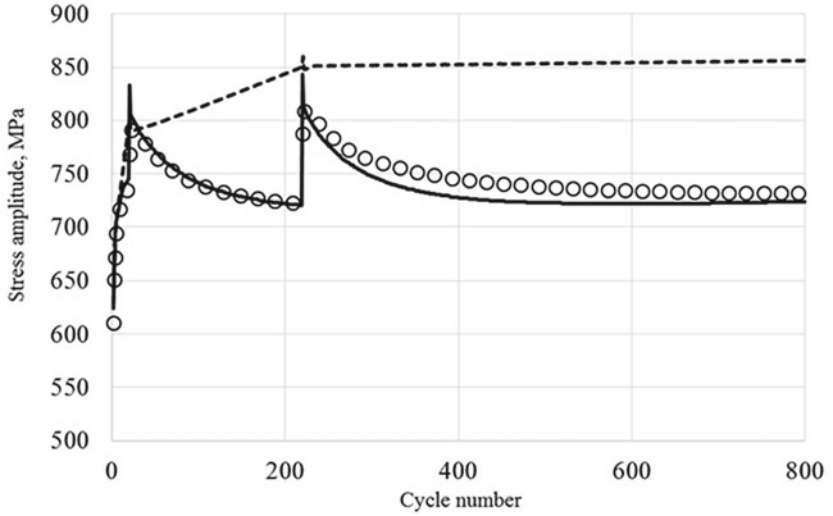

Fig. 6.6 Stress peak-to-peak amplitude

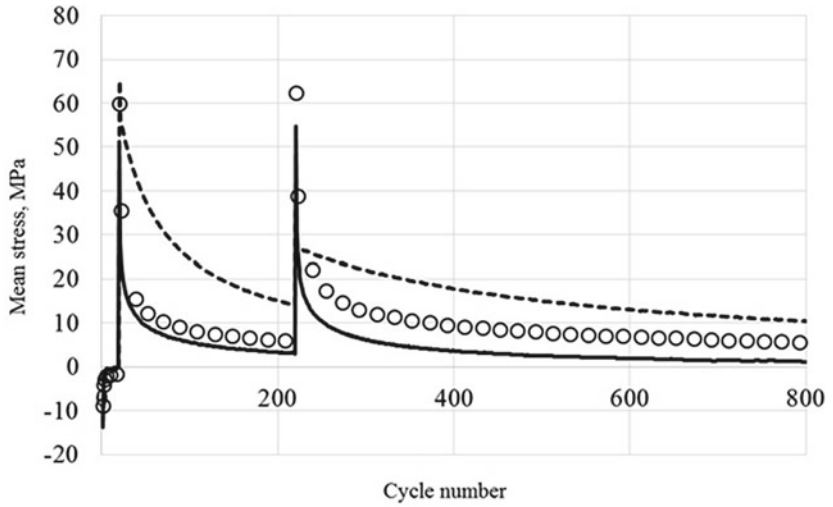

Fig. 6.7 Mean stress

The paper compares the results of computational and experimental studies of 12X18H10T stainless steel subjected to strain-controlled loading, a process consisting of a sequence of monotonic and cyclic loadings. Stress–strain state kinetics has been analyzed. Changes in the amplitude and mean stress of the cycle during cyclic loading have been dwelled upon. Computational and experimental results fit reliably.

The theory adequately describes the processes of how the kinetics, the amplitudes, and the mean cycle stress alter when subjecting a specimen to strain-controlled loading, which enables a more adequate description of stress-controlled loading, especially when loading is non-stationary and non-symmetric.

References

1. Abdel-Karim M (2009) Modified kinematic hardening rules for simulations of ratchetting. Int J Plast 25:1560–1587. https://doi.org/10.1016/j.ijplas.2008.10.004
2. Abdel-Karim M (2010) An evaluation for several kinematic hardening rules on prediction of multiaxial stress-controlled ratchetting. Int J Plast 26:711–730. https://doi.org/10.1016/j.ijplas.2009.10.002
3. Abdel-Karim M (2010) An extension for the Ohno-Wang kinematic hardening rules to incorporate isotropic hardening. Int J Plast 87:170–176. https://doi.org/10.1016/j.ijpvp.2010.02.003
4. Abdel-Karim M (2011) Effect of elastic modulus variation during plastic deformation on uniaxial and multiaxial ratchetting simulations. Int J Mech 30:11–21. https://doi.org/10.1016/j.euromechsol.2010.08.002
5. Bari S, Hassan T (2002) An advancement in cyclic plasticity modeling for multiaxial ratcheting simulation. Int J Plast 18:873–894. https://doi.org/10.1016/S0749-6419(01)00012-2
6. Besson J, Cailletaud G, Chaboche J-L, Forest S, Blétry M (2010) Non-linear mechanics of materials. Springer, Heidelberg
7. Bondar VSM (2004) Neuprugost'. Varianty teorii [Inelasticity. Variants of the theory]. Moscow, FIZMATLIT
8. Bondar VS, Danshin VV (2008) Plastichnost'. Proporcional'nye i neproporcional'nye nagruzhenija [Plasticity. Proportional and disproportionate loading]. Moscow, FIZMATLIT.
9. Bondar VS (2013) Inelasticity. Variants of the theory. New York, Begell House
10. Bondar VS, Danshin VV, Makarov DA, (2014) Mathematical modelling of deformation and damage accumulation under cyclic loading. PNRPU Mech Bull (2):125–152
11. Bondar VS, Danshin VV, Kondratenko AA (2015) Version of the theory of thermoplasticity. PNRPU Mech Bull (2):21–35. https://doi.org/10.15593/perm.mech/2015.2.02
12. Bondar VS, Danshin VV, Kondratenko AA (2016) Variant of thermoviscoplasticity theory. PNRPU Mech Bull (1):39–56.https://doi.org/10.15593/perm.mech/2016.1.03
13. Bondar VS, Abashev DR, Petrov VK (2017) Comparative analysis of variants of plasticity theories under cyclic loading. PNRPU Mech Bull 2:23–44. https://doi.org/10.15593/perm.mech/2017.2.02
14. Chaboche J-L (2008) A review of some plasticity and viscoplasticity constitutive theories. Int J Plast 24:1642–1692. https://doi.org/10.1016/j.ijplas.2008.03.009
15. Chaboche J-L, Kanouté P, Azzouz F (2012) Cyclic inelastic constitutive equations and their impact on the fatigue life predictions. Int J Plast 35:44–66. https://doi.org/10.1016/j.ijplas.2012.01.010
16. Hassan T, Taleb L, Krishna S (2008) Influence of non-proportional loading on ratcheting responses and simulations by two recent cyclic plasticity models. Int J Plast 24:1863–1889. https://doi.org/10.1016/j.ijplas.2008.04.008
17. Chang K-H, Jeon J-T, Lee C-H (2016) Effects of residual stresses on the uniaxial ratcheting behavior of a girth-welded stainless steel pipe. Int J Steel Struct 16:1381–1396. https://doi.org/10.1007/s13296-016-0072-1
18. Huang ZY, Chaboche JL, Wang QY, Wagner D (2014) Bathias C. Effect of dynamic strain aging on isotropic hardening in low cycle fatigue for carbon manganese steel. Mater Sci Eng A589:34–40. https://doi.org/10.1016/j.msea.2013.09.058

19. Kan Q, Kang G (2009) Constitutive model for uniaxial transformation ratcheting of superelastic NiTi shape memory alloy at room temperature. Int J Plast 26(3):441–465. https://doi.org/10.1016/j.ijplas.2009.08.005
20. Kang G, Kan Q (2007) Contitutive modeling for uniaxial time-dependent ratcheting of SS304 stainless steel. Mech Mater 39:488–499. https://doi.org/10.1016/j.mechmat.2006.08.004
21. Kapustin SA, Churilov YA, Gorohov VA (2015) Simulation of nonlinear deformation and fracture of structures under conditions of multifactorial effects based on FEM. N. Novgorod, Izd-vo NNGU
22. Kim JH, Kim D, Lee YS, Lee M-G, Chung K, Kim H-Y, Wagonere RH (2013) A temperature-dependent elasto-plastic constitutive model for magnesium alloy AZ31 sheets. Int J Plast 50:66–93. https://doi.org/10.1016/j.ijplas.2013.04.001
23. Lee C-H, Van Do VN, Chang K-H (2014) Analysis of uniaxial ratcheting behavior and cyclic mean stress relaxation of a duplex stainless steel. Int J Plast 62:17–33. https://doi.org/10.1016/j.ijplas.2014.06.008
24. Lee J-Y, Lee M-G, Barlat F, Bae G (2017) Piecewise linear approximation of nonlinear unloading-reloading behaviors using a multi-surface approach. Int J Plast 93:112–136. https://doi.org/10.1016/j.ijplas.2017.02.004
25. Mitenkov FM., Volkov IA, Igumnov LA, Kaplienko AV, Korotkikh IG, Panov VA (2015) Prikladnaia teoriia plastichnosti. Moscow, FIZMATLIT
26. Muhhamad W, Mohammadi M, Kang J, Mishra RK, Inal K (2015) An elasto-plastic constitutive model for evolving asymmetric/anisotropic hardening behavior of AZ31B and ZEK100 magnesium alloy sheets considering monotonic and reverse loading paths. Int J Plast 70:30–59. https://doi.org/10.1016/j.ijplas.2015.03.004
27. Qiao H, Agnew SR, Wu PD (2015) Modeling twinning and detwinning behavior of Mg alloy ZK60A during monotonic and cyclic loading. Int J Plast 65:61–84. https://doi.org/10.1016/j.ijplas.2014.08.010
28. Rahman SM, Hassan T, Corona E (2008) Evaluation of cyclic plasticity models in ratcheting simulation of straight pipes under cyclic bending and steady internal pressure. Int J Plast 24:1756–1791. https://doi.org/10.1016/j.ijplas.2008.02.010
29. Smith BD, Shih DS, McDowell DL (2018) Cyclic plasticity experiments and polycrystal plasticity modeling of three distinct Ti alloy microstructures. Int J Plast 101:1–23. https://doi.org/10.1016/j.ijplas.2013.10.004
30. Taleb L, Cailletaud G (2011) Cyclic accumulation of the inelastic strain in the 304L SS under stress control at room temperature: ratcheting or creep. Int J Plast 27(12):1936–1958. https://doi.org/10.1016/j.ijplas.2011.02.001
31. Taleb L (2013) About the cyclic accumulation of the inelastic strain observed in metals subjected to cyclic stress control. Int J Plast 43:1–19. https://doi.org/10.1016/j.ijplas.2012.10.009
32. Taleb L, Cailletaud G, Saï K (2014) Experimental and numerical analysis about the cyclic behavior of the 304L and 316L stainless steels at 350 °C. Int J Plast 61:32–48. https://doi.org/10.1016/j.ijplas.2014.05.006
33. Volkov IA, Igumnov LA (2007) Vvedenie v kontinualnuyu mehaniku povrezhdennoj sredy. [Introduction to conrinual mechanics of damaged media]. Moscow, FIZMATLIT
34. Volkov IA, Korotkikh JuG (2008) Uravnenija sostojanija vjazkouprugoplasticheskih sred s povrezhdenijami [The equation of state viscous elastoplastic media with injuries]. FIZMATLIT, Moscow
35. Volkov I.A., Igumnov L.A., Korotkikh Iu.G., 2015. Prikladnaia teoriia viazkoplastichnosti. N. Novgorod, Izd-vo NNGU.
36. Volkov IA, Igumnov LA, Tarasov IS, Shishulin DN, Markova MT (2018) Simulation of the fatigue life of polycrystalline structural alloys with block non-symmetrical low-cycle loading. Problemy Prochnosti i Plastichnosti 80(1):15–30
37. Yu C, Guozheng K, Song D, Kan Q (2015) Effect of martensite reorientation and reorientation-induced plasticity on multiaxial transformation ratchetting of super-elastic NiTi shape memory alloy: New consideration in constitutive model. Int J Plast 67:69–101. https://doi.org/10.1016/j.ijplas.2014.10.001

38. Zecevic M, Knezevic M (2015) A dislocation density based elasto-plastic self-consistent model for the prediction of cyclic deformation: application to AA6022-T4. Int J Plast 72:200–217. https://doi.org/10.1016/j.ijplas.2015.05.018
39. Zhu Y, Guozheng K, Yu C (2017) A finite cyclic elasto-plastic constitutive model to improve the description of cyclic stress-strain hysteresis loops. Int J Plast 95:191–215. https://doi.org/10.1016/j.ijplas.2017.04.009
40. Zhu Y, Kang G, Kan Q, Bruhns OT (2014) Logarithmic stress rate based constitutive model for cyclic loading in finite plasticity. Int J Plast 54:34–55. https://doi.org/10.1016/j.ijplas.2013.08.004